Intergalactic medium heating by dark matter

Ripamonti, E.; Mapelli, M.; Ferrara, A.

Published in:
Monthly Notices of the Royal Astronomical Society

DOI:
10.1111/j.1365-2966.2006.11222.x

Publication date:
2007

Mon. Not. R. Astron. Soc. **374,** 1067–1077 (2007) doi:10.1111/j.1365-2966.2006.11222.x

Intergalactic medium heating by dark matter

E. Ripamonti,[1⋆] M. Mapelli[2] and A. Ferrara[2]

[1]*Kapteyn Astronomical Institute, University of Groningen, Postbus 800, 9700 AV Groningen, The Netherlands*
[2]*SISSA, International School for Advanced Studies, Via Beirut 4, 34100 Trieste, Italy*

Accepted 2006 October 20. Received 2006 October 2; in original form 2006 June 8

ABSTRACT

We derive the evolution of the energy deposition in the intergalactic medium (IGM) by dark matter (DM) decays/annihilations for both sterile neutrinos and light dark matter (LDM) particles. At $z > 200$ sterile neutrinos transfer a fraction $f_{\rm abs} \sim 0.5$ of their rest mass energy into the IGM; at lower redshifts this fraction becomes $\lesssim$0.3 depending on the particle mass. The LDM particles can decay or annihilate. In both the cases $f_{\rm abs} \sim 0.4$–0.9 at high (>300) redshift, dropping to ≈0.1 below $z = 100$. These results indicate that the impact of DM decays/annihilations on the IGM thermal and ionization history is less important than previously thought. We find that sterile neutrinos (LDM) decays are able to increase the IGM temperature by $z = 5$ at most up to 4 K (100 K), about 50–200 times less than predicted by estimates based on the assumption of complete energy transfer to the gas.

Key words: neutrinos – ISM: evolution – dark matter.

1 INTRODUCTION

According to 3-yr *WMAP* (*Wilkinson Microwave Anisotropy Probe*) results (Spergel et al. 2006), the dark matter (DM) constitutes about 20 per cent of the cosmic energy density. However, the nature of such elusive component remains unclear.

As proposed DM candidates might induce drastically different evolutionary effects depending on their properties (e.g. velocity dispersion), one hopes to be able to select suitable DM candidates from the comparison between their predicted effects and observations.

Potentially important cosmological effects might be induced if DM particles either decay or annihilate, as predicted by fundamental physics theories. For example, sufficiently light DM particles (mass $\lesssim$100 MeV; Boehm et al. 2004; Ascasibar et al. 2006) can annihilate, or decay into lighter particles (Hooper & Wang 2004; Picciotto & Pospelov 2005; Ascasibar et al. 2006) remaining good DM candidates. The products of DM decays/annihilations can be photons, neutrinos, electron–positron pairs and/or more massive particles, depending on the mass of the progenitor.

The decay/annihilation of DM particles into e^+–e^- pairs has been recently invoked to explain the observation, by the SPI spectrometer aboard ESA's *INTEGRAL* satellite, of an excess in the 511-keV line emission from the Galactic bulge (Knödlseder et al. 2005). Although exotic, this idea has triggered many theoretical studies (Boehm et al. 2004; Hooper & Wang 2004; Kasuya & Takahashi 2005; Kawasaki & Yanagida 2005; Picciotto & Pospelov 2005; Ascasibar et al. 2006; Cassé & Fayet 2006), aimed at constraining DM properties through SPI/*INTEGRAL* observations.

⋆E-mail: ripa@astro.rug.nl

The products of decays and/or annihilations are expected to interact with the intergalactic medium (IGM), transferring part of their energy. If so, DM decays and annihilations might change the IGM thermal/ionization history in a sensible and detectable way. Various flavours of this mechanism have been investigated in a considerable number of studies (Chen & Kamionkowski 2004; Hansen & Haiman 2004; Pierpaoli 2004; Mapelli & Ferrara 2005; Padmanabhan & Finkbeiner 2005; Biermann & Kusenko 2006; Mapelli, Ferrara & Pierpaoli 2006, hereafter MFP06; Zhang et al. 2006).

The above studies, though, made the simplifying assumptions that either (i) the energy injected by DM decays/annihilation is *entirely* absorbed by the IGM (Hansen & Haiman 2004; Pierpaoli 2004; Biermann & Kusenko 2006; MFP06) or (ii) leave the absorption efficiency as a free parameter (Padmanabhan & Finkbeiner 2005; Zhang et al. 2006) or (iii) make a partial treatment of the physical processes responsible for the energy redistribution (Chen & Kamionkowski 2004; Mapelli & Ferrara 2005).

In this paper we model in detail, for the first time, the physical processes governing the interaction between the IGM and the decay/annihilation products, and we derive the fraction of energy actually absorbed (Section 2). We restrict our analysis to the case in which the decay/annihilation products are photons, electron–positron pairs or neutrinos (which are assumed to have negligible interactions with matter), because of the uncertainties in modelling the cascade associated with more massive product particles. For photons (Section 2.1) we include the effects of Compton scattering and photoionization; for pairs, the relevant processes are inverse Compton scattering, collisional ionizations and positron annihilations (Section 2.2).

Our model exhaustively describes the behaviour of relatively light DM candidates (i.e. warm and cold DM particles with mass lower

than ∼100 MeV), whose only decay/annihilation products are photons, pairs and neutrinos. As an application, we explore the effects of sterile neutrinos (mass 2–50 keV) and of viable light dark matter particles (LDM; mass 1–10 MeV) on the IGM thermal and ionization history (Section 3).

We adopt the best-fitting cosmological parameters after the 3-yr *WMAP* results (Spergel et al. 2006), i.e. $\Omega_{\rm b} = 0.042$, $\Omega_{\rm M} = 0.24$, $\Omega_{\rm DM} \equiv \Omega_{\rm M} - \Omega_{\rm b} = 0.198$, $\Omega_\Lambda = 0.76$, $h = 0.73$ and $H_0 = 100\,h\,{\rm Mpc^{-1}\,km\,s^{-1}}$.

2 ENERGY INJECTION IN THE IGM

We consider the case of DM decays and annihilations resulting in the direct production of photons, electron–positron pairs and/or neutrinos, and study the absorption of the energy of such particle products by the IGM.

Some fraction of the energy of the newly created particles is immediately absorbed; the remainder will remain in the form of a *background*, eventually absorbed at later times.

In practice, at each redshift z, it is convenient to distinguish the particles which were produced by DM decays and/or annihilations according to their 'production redshift' z' and energy E. We define $n(z, z')$ as the number (per baryon) of product particles which at redshift z can still inject energy in the IGM, and were produced at redshift $z' \geqslant z$. Their energy spectrum is $({\rm d}n/{\rm d}E)(z, z', E)$.

The rate of energy absorption per baryon in the IGM at redshift z is the sum of the contributions of all 'product particles', obtained by the integration over production redshift and energy:

$$\epsilon(z) = \int_z^{z_{\rm max}} {\rm d}z' \int {\rm d}E\, \frac{{\rm d}n}{{\rm d}E}(z, z', E) E \phi(z, E), \tag{1}$$

where $\phi(z, E)$ is the fraction of the energy E of a particle which is absorbed by the IGM per unit time, calculated at redshift z. We assume $z_{\rm max} = 1100$, which is approximately the redshift of the last scattering surface (Spergel et al. 2006).

However, using equation (1) is both complicated and unnecessary: in fact, we know that the energy spectrum of 'fresh' DM decay/annihilation products is essentially mono-energetic, and it is reasonable to expect that it will remain peaked at the average energy. Therefore, we assume that the energy integration inside equation (1) can be safely eliminated by using the average energy $\bar{E}(z, z')$ of the particles,

$$\bar{E}(z, z') = \frac{1}{n(z, z')} \int {\rm d}E \frac{{\rm d}n}{{\rm d}E}(z, z', E) E, \tag{2}$$

so that equation (1) becomes

$$\epsilon(z) = \int_z^{z_{\rm max}} {\rm d}z'\, n(z, z') \bar{E}(z, z') \phi[z, \bar{E}(z, z')]. \tag{3}$$

The evolution of $n(z, z')$, $\bar{E}(z, z')$ and $\phi(z, E)$ obviously depends on the type of DM decay/annihilation product we are considering. If the product particles are neutrinos $\phi_\nu(z, E) = 0$; the cases of photons and electron–positron pairs are discussed in the following sections.

2.1 Photons

If the DM decays or annihilations result in the production of photons, the only two important energy loss mechanisms in the considered energy and redshift ranges ($25\,{\rm eV} \lesssim E \lesssim 50\,{\rm MeV}$; $z \lesssim 1000$) are ionizations and Compton scattering on cold matter (see Zdziarski & Svensson 1989, hereafter ZS89). All the energy lost by the photons is absorbed by the IGM, so we can write

$$\phi_\gamma(z, E) = \phi_{\gamma,{\rm ion}}(z, E) + \phi_{\gamma,{\rm com}}(z, E). \tag{4}$$

The photoionization term can be expressed as

$$\phi_{\gamma,{\rm ion}}(z, E) = \frac{\sigma_{\rm He+H}(E)}{16} N_{\rm b}(z) c, \tag{5}$$

where $N_{\rm b}(z) \simeq 2.5 \times 10^{-7}\,(1+z)^3 (\Omega_{\rm b} h^2/0.0224)\,{\rm cm^{-3}}$ is the number density of the baryons at redshift z, and

$$\sigma_{\rm He+H}(E) = \sigma_{\rm He} + 12\sigma_{\rm H} \simeq 5.1 \times 10^{-20} \left(\frac{E}{250\,{\rm eV}}\right)^{-p}\,{\rm cm^2} \tag{6}$$

(with $p = 3.30$ for $E > 250\,{\rm eV}$, $p = 2.65$ for $25 \leqslant E \leqslant 250\,{\rm eV}$) is the photoionization absorption cross-section per helium atom of the cosmological mixture of H and He (see equation 3.2 of ZS89). Equation (5) implicitly assumes that the IGM is mostly neutral, which is true between the hydrogen recombination at $z \simeq 1100$, and its reionization at $z \sim 6$–15.

The Compton scattering term is

$$\phi_{\gamma,{\rm com}}(z, E) = [\sigma_{\rm T}\, \xi\, g(\xi)] N_{\rm e}(z) c, \tag{7}$$

where $\xi \equiv E/(m_{\rm e}c^2)$, $N_{\rm e}(z)$ is the electron number density and the product $\sigma_{\rm T}\xi g(\xi)$ gives the average fraction of energy which is lost by a photon for each electron on its path [$\sigma_{\rm T} \simeq 6.65 \times 10^{-25}\,{\rm cm^{-2}}$ is the Thomson cross-section; see equation 4.9 of ZS89 for the definition of the function $g(\xi)$]. In equation (7) the electron number density accounts for both free and bound electrons, as the energy losses due to Compton scattering only become important when E is so high that the interaction is insensitive to whether an electron is bound or free (Chen & Kamionkowski 2004). Then, $N_{\rm e}(z) = [(1 + 2f_{\rm He})/(1 + 4f_{\rm He})]\, N_{\rm b}(z) \simeq 0.88\, N_{\rm b}(z)$, where $f_{\rm He} = 0.0789$ is the helium-to-hydrogen number ratio.

We assume that the energy transfer through ionization results in a photon loss, whereas Compton scatterings reduce the average energy of the photons without changing their number. So, for $z < z'$ the equations for the cosmological evolution of $n(z, z')$ and $E(z, z')$ are

$$\frac{n(z + {\rm d}z, z')}{n(z, z')} = 1 - \phi_{\gamma,{\rm ion}}[z, \bar{E}(z, z')] \frac{{\rm d}t}{{\rm d}z} {\rm d}z, \tag{8}$$

$$\frac{\bar{E}(z + {\rm d}z, z')}{\bar{E}(z, z')} = 1 - \phi_{\gamma,{\rm com}}[z, \bar{E}(z, z')] \frac{{\rm d}t}{{\rm d}z} {\rm d}z + \frac{{\rm d}z}{1+z}, \tag{9}$$

where the energy equation also keeps into account the cosmological redshifting of photons (also note that ${\rm d}t/{\rm d}z$ is negative).

These equations need to be supplemented with the injection of new photons at each redshift $z = z'$:

$$n(z' + {\rm d}z, z') = \zeta_1 \dot{n}_{\rm DM}(z') \frac{{\rm d}t}{{\rm d}z} {\rm d}z, \tag{10}$$

$$\bar{E}(z' + {\rm d}z, z') = \zeta_2 m_{\rm DM} c^2 \left(1 + \frac{{\rm d}z}{1+z}\right), \tag{11}$$

where $\dot{n}_{\rm DM}(z')$ is the rate of decrease of the number of DM particles per baryon at redshift z' and $m_{\rm DM}$ is the mass of a DM particle (see Section 2.3). ζ_1 and ζ_2 are numerical coefficients which depend on the considered DM particle and on the details of its decay or annihilation.

2.2 Pair production

Even if the loss of kinetic energy from electrons and positrons can be treated exactly in the same way, the annihilation probability is negligible for the electrons, but must be kept into account for the positrons. For this reason, when DM decays/annihilations result in the production of an electron–positron pair, it is useful to distinguish between electrons and positrons.

In the case of annihilations we neglect other processes, such as the internal Bremsstrahlung, which affect $\epsilon(z)$ only in a minor way (see Appendix A).

Note that in the following we will always include the rest energy $m_e c^2$ as part of the energy E of the particle.

2.2.1 Electrons

Electrons can transfer their kinetic energy to the IGM through collisional ionizations and ionizations by inverse Compton up-scattered cosmic microwave background (CMB) photons. Here we neglect the energy loss through synchrotron radiation, because the inverse Compton mechanism is more efficient by a factor $U_{\rm CMB}/U_B$ (where $U_{\rm CMB}$ and U_B are the energy densities of the CMB and of the magnetic field, respectively), which is $\gg 1$ unless unrealistically strong magnetic fields ($B \gtrsim 10^{-5}$ G) are assumed to exist in the IGM at $z \geqslant 5$.

It is necessary to remark that photons produced by the inverse Compton mechanism are not necessarily absorbed by the IGM, and we must distinguish between the fractional energy loss rate by electrons,

$$\Phi_{\rm e-}(z, E) = \Phi_{\rm e,ion}(z, E) + \Phi_{\rm e,com}(z, E), \tag{12}$$

and the fractional energy loss rate actually absorbed by the IGM,

$$\phi_{\rm e-}(z, E) = \phi_{\rm e,ion}(z, E) + \phi_{\rm e,com}(z, E). \tag{13}$$

The ionization losses are completely absorbed by the IGM, so that

$$\begin{aligned}\phi_{\rm e,ion}(z, E) = \Phi_{\rm e,ion}(z, E) \simeq \frac{v}{E}\frac{2\pi e^4}{m_e v^2} \\ \times\left\{ Z_{\rm H} N_{\rm H}(z) \left[\ln\left(\frac{m_e v^2 \gamma^2 T_{\rm max,H}}{2E_{\rm th,H}^2} \right) + \mathcal{D}(\gamma) \right] \right. \\ \left. + Z_{\rm He} N_{\rm He}(z) \left[\ln\left(\frac{m_e v^2 \gamma^2 T_{\rm max,He}}{2E_{\rm th,He}^2} \right) + \mathcal{D}(\gamma) \right] \right\},\end{aligned} \tag{14}$$

where v and e are the velocity and charge of the electron, $\gamma = E/(m_e c^2)$ is the electron Lorentz factor, $E_{\rm th,H} = 13.59$ eV ($E_{\rm th,He} = 24.6$ eV) is the hydrogen (helium) ionization threshold, $Z_{\rm H} = 1$ ($Z_{\rm He} = 2$) is the hydrogen (helium) atomic number, $N_{\rm H}(z) = N_{\rm b}(z)/(1 + 4f_{\rm He})$ is the H number density, $N_{\rm He}(z) = N_{\rm b}(z) f_{\rm He}/(1 + 4f_{\rm He})$ is the He number density, $\mathcal{D}(\gamma) = 1/\gamma^2 - (2/\gamma - \frac{1}{\gamma^2})\ln 2 + (1/8)(1 - 1/\gamma)^2$ and

$$\begin{aligned}T_{\rm max,H} &= \frac{2\gamma^2 m_{\rm H}^2 m_e v^2}{m_e^2 + m_{\rm H}^2 + 2\gamma m_e m_{\rm H}}, \\ T_{\rm max,He} &= \frac{2\gamma^2 (4m_{\rm H})^2 m_e v^2}{m_e^2 + (4m_{\rm H})^2 + 2\gamma m_e (4m_{\rm H})}\end{aligned} \tag{15}$$

(cf. Longair 1992, and also Lang 1999 and Chen & Kamionkowski 2004).

The total Compton fractional losses are given by

$$\Phi_{\rm e,com}(z, E) = \left(\frac{1}{E}\right)\frac{4}{3}\sigma_{\rm T} c a_{\rm rad} T_{\rm CMB}(z)^4 (\gamma^2 - 1), \tag{16}$$

where $a_{\rm rad} \simeq 7.56 \times 10^{-15}$ erg cm^{-3} K^{-4} is the Stefan–Boltzmann constant for the radiation energy density, and $T_{\rm CMB}(z) \simeq 2.726(1 + z)$ K is the temperature of the CMB radiation at redshift z (cf. Rybicki & Lightman 1979; Longair 1992); the fractional loss rate that is actually absorbed by the IGM is

$$\phi_{\rm e,com}(z, E) = \Phi_{\rm e,com}(z, E)\frac{\gamma^2}{\gamma^2 - 1}\int_{\nu(\gamma)}^{\infty} {\rm d}\nu \frac{4\pi B_\nu[T_{\rm CMB}(z)]}{a_{\rm rad} c T_{\rm CMB}(z)^4}, \tag{17}$$

where $B_\nu(T)$ is the Planck function for blackbody radiation at temperature T, and

$$\nu(\gamma) = \frac{3E_{\rm th,H}}{4h_{\rm P}\gamma^2}, \tag{18}$$

where $h_{\rm P}$ is the Planck constant. The correction to $\Phi_{\rm e,com}$ introduced in equation (17) amounts to neglecting photons with pre-interaction frequencies below $\nu(\gamma)$. This is necessary because on average the post-interaction energies of such photons are below $E_{\rm ion,H}$, so that they are hardly absorbed by the IGM.[1]

As in the case of photons, we assume that ionization energy losses lead to the disappearance of electrons, whereas Compton losses reduce the average energy of the surviving electrons. Therefore, the equations describing the evolution of the energetic electrons coming from decays and annihilations are quite similar to those we used for photons. For redshifts $z < z'$ we have

$$\frac{n_{\rm e-}(z + {\rm d}z, z')}{n_{\rm e-}(z, z')} = 1 - \Phi_{\rm e,ion}[z, \bar{E}_{\rm e-}(z, z')]\frac{{\rm d}t}{{\rm d}z}{\rm d}z, \tag{19}$$

$$\frac{\bar{E}_{\rm e-}(z + {\rm d}z, z')}{\bar{E}_{\rm e-}(z, z')} = 1 - \Phi_{\rm e,com}[z, \bar{E}_{\rm e-}(z, z')]\frac{{\rm d}t}{{\rm d}z}{\rm d}z, \tag{20}$$

whereas the injection of new electrons is described by

$$n_{\rm e-}(z' + {\rm d}z, z') = \zeta_1 \dot{n}_{\rm DM}(z')\frac{{\rm d}t}{{\rm d}z}{\rm d}z, \tag{21}$$

$$\bar{E}_{\rm e-}(z' + {\rm d}z, z') = \zeta_2 m_{\rm DM} c^2, \tag{22}$$

where, again, ζ_1 and ζ_2 depend on the details of the considered decaying or annihilating particle.

2.2.2 Positrons

In addition to the energy loss mechanisms of electrons, decay produced positrons can also annihilate with thermal electrons in the surrounding gas. The fractional energy loss due to the annihilations of positrons of energy E is

$$\Phi_{\rm ann}(E) = v N_{\rm e}(z)\,\sigma_{\rm ann}(E), \tag{23}$$

where the annihilation cross-section $\sigma_{\rm ann}$ is (cfr. Beacom & Yüksel 2006)

$$\begin{aligned}\sigma_{\rm ann}(E) = \frac{3\sigma_{\rm T}}{8(\gamma + 1)} \\ \times \left[\frac{\gamma^2 + 4\gamma + 1}{\gamma^2 - 1}\ln(\gamma + \sqrt{\gamma^2 - 1}) - \frac{\gamma + 3}{\sqrt{\gamma^2 - 1}} \right].\end{aligned} \tag{24}$$

Every annihilation emits two photons, each of energy $E_\gamma \sim (1/2)(E + m_e c^2)$, as it involves a positron of energy E and an

[1] Lyman α opacity generally results only in the scattering of the photon, rather than in its absorption, and only a small fraction of the energy is absorbed (Furlanetto & Pritchard 2006).

electron whose energy is likely to be close to $m_e\ c^2$. Such photons are absorbed only if the optical depth they encounter is sufficiently high. Here we do not follow their radiative transfer in detail, and simply assume that the fractional energy loss which actually goes in the IGM is

$$\phi_{\rm ann}(z,\,E) = \Phi_{\rm ann}(z,\,E) f_1 \left[1 - {\rm e}^{-\tau_\gamma(z,E_\gamma)}\right] \tag{25}$$

with

$$\tau_\gamma(z,\,E_\gamma) = \frac{f_2}{H(z)} \phi_{\gamma,{\rm com}}(z,\,E_\gamma), \tag{26}$$

where $H(z)$ is the expansion rate of the Universe at redshift z, and $\phi_{\gamma,{\rm com}}(z,\,E_\gamma)$ is the Compton fractional energy loss of a photon of energy E_γ, as defined in equation (7). Equation (26) represents a fraction f_2 of the optical depth encountered by a photon of energy E_γ emitted at redshift z and travelling a Hubble radius, assuming that the baryonic density does not vary. The parameters $f_1 = 0.91$ and $f_2 = 0.6$ have been chosen in order to maximize the agreement between a full radiative transfer treatment and our simple approximation.

Equation (25) implies that annihilation energy loss is particularly efficient for positrons with very low kinetic energy, as $\sigma_{\rm ann}(E) \propto (\gamma - 1)^{-1/2}$ when $E \approx m_e c^2$ (and γ tends to 1).

For this reason, it is convenient to separate positrons in two different groups: 'fast' positrons (which effectively lose energy through ionizations, inverse Compton, and annihilations) and 'thermal' positrons (whose kinetic energy is so low that annihilations are their only energy loss mechanism).

The treatment of fast positrons is very similar to that of electrons: their fractional energy loss rate is

$$\Phi_{\rm e+,f}(z,\,E) = \Phi_{\rm e,ion}(z,\,E) + \Phi_{\rm e,com}(z,\,E) + \Phi_{\rm ann}(z,\,E), \tag{27}$$

and the fractional energy loss rate actually absorbed by the IGM is

$$\phi_{\rm e+,f}(z,\,E) = \phi_{\rm e,ion}(z,\,E) + \phi_{\rm e,com}(z,\,E) + \phi_{\rm ann}(z,\,E), \tag{28}$$

where the ionization and Compton terms are exactly the same as in the case of electrons.

Their evolution is described by the equations which are simple modifications of those given for electrons, taking annihilations into account

$$\frac{n_{\rm f}(z + {\rm d}z,\,z')}{n_{\rm f}(z,\,z')} = 1 - [\Phi_{\rm e,ion}(z,\,\bar{E}_{\rm f}(z,\,z')) + \Phi_{\rm ann}(z,\,\bar{E}_{\rm f}(z,\,z'))]\frac{{\rm d}t}{{\rm d}z}{\rm d}z, \tag{29}$$

$$\frac{\bar{E}_{\rm f}(z + {\rm d}z,\,z')}{\bar{E}_{\rm f}(z,\,z')} = 1 - \Phi_{\rm e,com}(z,\,\bar{E}_{\rm f}(z,\,z'))\frac{{\rm d}t}{{\rm d}z}{\rm d}z, \tag{30}$$

where the 'f' subscripts refer to 'fast' positrons (e.g. $\bar{E}_{\rm f}$ is the average energy of the fast positrons). Their injection rate and average energy at injection are identical to those given in equations (21) and (22) for electrons: $n_{\rm f}(z' + {\rm d}z,\,z') = n_{\rm e-}(z' + {\rm d}z,\,z')$, $\bar{E}_{\rm f}(z' + {\rm d}z,\,z') = \bar{E}_{\rm e-}(z' + {\rm d}z,\,z')$.

The fractional energy losses (total and absorbed by the IGM) of thermal positrons are simply

$$\Phi_{\rm e+,t}(z,\,E) = \Phi_{\rm ann}(z,\,E), \tag{31}$$

$$\phi_{\rm e+,t}(z,\,E) = \phi_{\rm ann}(z,\,E); \tag{32}$$

their evolution equations are

$$n_{\rm t}(z + {\rm d}z,\,z') = n_{\rm t}(z,\,z')[1 - \Phi_{\rm ann}(z,\,\bar{E}_{\rm t}(z))] + n_{\rm f}(z,\,z')\Phi_{\rm e,ion}(z,\,\bar{E}_{\rm f}(z,\,z')), \tag{33}$$

$$\bar{E}_{\rm t}(z) = m_e c^2 + \frac{3}{2} k_{\rm B} T_{\rm IGM}(z), \tag{34}$$

where the 't' subscripts refer to 'thermal' positrons, $k_{\rm B}$ is the Boltzmann constant and $T_{\rm IGM}(z)$ is the temperature of the IGM at redshift z. We take the injection rate to be simply $n_{\rm t}(z',\,z') = 0$, as positrons are naturally 'fast' when they are created.

In practice, these equations assume that the only mechanism which leads to the disappearance of a positron is its annihilation; instead, ionization energy losses simply turn a fast positron into a thermal one.

2.3 The absorbed energy fraction

The energy injection rate per baryon resulting from the integration of equation (3) can be expressed in the form of the fraction $f_{\rm abs}$ of the total energy released by the DM which is absorbed by the IGM:

$$f_{\rm abs}(z) = \frac{\epsilon(z)}{\dot{n}_{\rm DM}(z) m_{\rm DM} c^2}. \tag{35}$$

In the case of decaying DM, $\dot{n}_{\rm DM}$ (which we defined as the decrease rate of the number of DM particles per baryon) is given by

$$\dot{n}_{\rm DM}(z) = \frac{n_{\rm DM,0}}{\tau_{\rm DM}} {\rm e}^{(t(0)-t(z))/\tau_{\rm DM}} \simeq \frac{n_{\rm DM,0}}{\tau_{\rm DM}}, \tag{36}$$

where $n_{\rm DM,0}$ is the number of DM particles per baryon at present, $\tau_{\rm DM}$ is the lifetime of a DM particle, and $t(0)$ and $t(z)$ are the ages of the Universe at present and at redshift z, respectively. The leftmost equality is valid when $\tau_{\rm DM} \gg t(0)$, which is generally the case.

Instead, in the case of annihilating DM, $\dot{n}_{\rm DM}$ is

$$\dot{n}_{\rm DM}(z) \simeq \frac{1}{2} n_{\rm DM,0}^2\, N_{\rm b}(0)\, \langle \sigma\ v \rangle (1 + z)^3, \tag{37}$$

where $\langle \sigma\, v \rangle$ is the thermally averaged annihilation cross-section; the 1/2 factor is due to two reasons: first, the DM is split in half between particles and antiparticles, and this needs to be accounted by introducing a correction factor of 1/4. However, this must be multiplied by 2, as each annihilation involves two DM particles.

The definition of the absorbed fraction,[2] $f_{\rm abs}$, given in equation (35) is such that it can be easily plugged into the equations commonly used in studies concerned with decaying and annihilating DM (e.g. Padmanabhan & Finkbeiner 2005; Zhang et al. 2006). A second advantage of the $f_{\rm abs}$ notation is that it is independent of uncertain quantities such as $\tau_{\rm DM}$ and $\langle \sigma\, v \rangle$.

3 APPLICATIONS

The rate of energy absorption per baryon, $\epsilon(z)$, that was derived in the previous section, can be used to improve our knowledge of the effects of DM decays/annihilations on cosmic reionization and heating. In fact, most of the previous works (Chen & Kamionkowski 2004; Padmanabhan & Finkbeiner 2005; MFP06; Zhang et al. 2006) derived only an upper limit to these effects, by assuming that all the energy emitted during the decay/annihilation is absorbed, or considering the energy absorbed fraction, $f_{\rm abs}(z)$, as a free (and mostly unknown) parameter.

[2] We remark that the term 'absorbed fraction' might be slightly misleading, as it is theoretically possible to have $f_{\rm abs} > 1$ in scenarios where $\epsilon(z)$ is dominated by the absorption from particles in the 'background', rather than from the ones which were produced recently. This might happen, for example, when $\dot{n}_{\rm DM}$ decreases very rapidly.

Now, we have an estimate of $\epsilon\ (z)$ and $f_{\rm abs}(z)$ which accounts for all the important physics involved, and we can use it to derive the effective influence of DM decays/annihilations on the cosmic reionization and heating. For this purpose, we ran the public version of the code RECFAST (Seager, Sasselov & Scott 1999, 2000), modified to account for the energy injection from DM decays and annihilations. The adopted procedure is mostly the same as described in MFP06. Here, we briefly summarize the most important assumptions of this method, pointing out the improvements of our present treatment.

The IGM is heated, excited and ionized by the energy input due to DM decays/annihilations. It is important to note that the fraction of the absorbed energy going into each one of these components is quite unrelated to how the energy was deposited in the IGM in the first place. For example, if a keV photon ionizes an atom, the resulting electron will generate a cascade of collisions, and the energy of the photon will go not only into ionizations, but also into excitations and heating.

In order to treat this process, we assume that a fraction $(1 - x)/3$ (where x is the ionization fraction) of the energy absorbed by the IGM contributes to the ionizations (Chen & Kamionkowski 2004), and that a fraction $\mathcal{F}(x) = \tilde{C}[1 - (1 - x^{\tilde{a}})^{\tilde{b}}]$ (where $\tilde{C} = 0.9971$, $\tilde{a} = 0.2663$ and $\tilde{b} = 1.3163$; Shull & van Steenberg 1985) goes into heating. This definition of $\mathcal{F}(x)$ comes directly from a fit to the results of the simulations given by Shull & van Steenberg (1985), replacing the significantly less accurate form that is used in Chen & Kamionkowski (2004) and in MFP06.

The evolution equations in RECFAST have been modified adding the DM energy injection terms:

$$-\delta\left(\frac{{\rm d}x_{\rm H}}{{\rm d}z}\right) = \frac{\epsilon(z)}{E_{\rm th,H}}\,\frac{1+4f_{\rm He}}{1+f_{\rm He}}\,\frac{1-x_{\rm H}}{3}\,\mathcal{E}, \tag{38}$$

$$-\delta\left(\frac{{\rm d}x_{\rm He}}{{\rm d}z}\right) = \frac{\epsilon(z)}{E_{\rm th,He}}\,\frac{1+4f_{\rm He}}{1+f_{\rm He}}\,\frac{1-x_{\rm He}}{3}\,\mathcal{E}, \tag{39}$$

$$-\delta\left(\frac{{\rm d}T_{\rm IGM}}{{\rm d}z}\right) = \frac{2\,\epsilon(z)}{3\,k_{\rm B}}\,\frac{1+4f_{\rm He}}{1+f_{\rm He}} \times \frac{\mathcal{F}(x_{\rm H}) + f_{\rm He}\,\mathcal{F}(x_{\rm He})}{1+f_{\rm He}}\,\mathcal{E}, \tag{40}$$

where $x_{\rm H}(x_{\rm He})$ is the ionized fraction of hydrogen (helium) atoms, and $\mathcal{E} \equiv [H(z)\,(1+z)]^{-1}$. These equations are slightly different from the ones used e.g. in Padmanabhan & Finkbeiner (2005) because in our case $\epsilon(z)$ is the energy absorption rate *per baryon*, rather than *per hydrogen atom*.

We apply this formalism to two different DM candidates, i.e. sterile neutrinos and LDM, which are expected to have the maximum impact on reionization and heating (MFP06). In the case of sterile neutrinos, only the decay process is allowed (see Section 3.1). For LDM particles (Section 3.2) we discuss both the decay and the annihilation process.

We do not consider heavier DM candidates (such as gravitinos or neutralinos) because MFP06 have already showed that, even assuming $f_{\rm abs} = 1$, their contribution to reionization and heating is completely negligible, and there is no point in extending our formalism in order to account for them.

3.1 Sterile neutrinos

Sterile neutrinos are one of the most popular warm DM candidates (Colombi, Dodelson & Widrow 1996; Sommer-Larsen & Dolgov 2001). Their existence is predicted by the standard oscillation theory and required by various extensions of the Minimal Standard Model, such as the νMSM (Shaposhnikov 2006 and references therein). They are massive; so they can decay following different channels. In this paper we will consider only the so-called radiative decay, i.e. the decay of a sterile neutrino into an active neutrino and a photon.

The mass of radiatively decaying sterile neutrinos can be constrained by the absence of any detection of X-ray lines consistent with photons due to sterile neutrino decays in nearby galaxy clusters (Abazajian, Fuller & Tucker 2001; Abazajian 2006; Abazajian & Koushiappas 2006; Boyarsky et al. 2006b). Recently, Watson et al. (2006) applied the same method to the X-ray emission from the Andromeda galaxy, finding an upper limit

$$m_{\nu\,\rm s}c^2 \lesssim 2.1\,{\rm keV}\left(\frac{\sin^2 2\theta}{10^{-7}}\right)^{-0.213}, \tag{41}$$

where θ is the mixing angle. This limit is valid for masses $m_{\nu\,\rm s}\,c^2 \lesssim 24\,{\rm keV}$. The most stringent constraints for masses $m_{\nu\,\rm s}\,c^2 > 24\,{\rm keV}$ come from the comparison between the unresolved X-ray background and the expected contribution from sterile neutrino decays (Mapelli & Ferrara 2005; Boyarsky et al. 2006a):

$$m_{\nu\,\rm s}c^2 \lesssim 25\,{\rm keV}\left(\frac{\Omega_{\rm DM}}{0.198}\right)^{-0.2}\left(\frac{\sin^2 2\theta}{1.55\times10^{-11}}\right)^{-0.2}. \tag{42}$$

For masses lower than $\sim$3.5 keV the main constraints arise from the positivity of the lepton number.

On the other hand, the study of matter power spectrum fluctuations provides a conservative lower limit of $m_{\nu\,\rm s}c^2 \gtrsim 2\,{\rm keV}$ (Viel et al. 2005), even if more recent estimates significantly increase this lower limit ($m_{\nu\,\rm s}c^2 \gtrsim 14\,{\rm keV}$, Seljak et al. 2006; $m_{\nu\,\rm s}\,c^2 \gtrsim 10\,{\rm keV}$, Viel et al. 2006). It is worth noting that these lower limits are independent of the mixing angle.

According to the X-ray observational constraints discussed above, the minimum possible lifetime for sterile neutrino radiative decays is (Mapelli & Ferrara 2005; MFP06)

$$\tau_{\rm DM} = 2.23\times10^{27}\,{\rm s}\left(\frac{m_{\nu\,\rm s}\,c^2}{10\,{\rm keV}}\right)^{-5}\left(\frac{6.6\times10^{-11}}{\sin^2 2\theta}\right), \tag{43}$$

if $3.5 \lesssim m_{\nu\,\rm s}\,c^2/{\rm keV} \lesssim 24$, and

$$\tau_{\rm DM} = 9.67\times10^{25}\,{\rm s}\left(\frac{m_{\nu\,\rm s}c^2}{25\,{\rm keV}}\right)^{-5}\left(\frac{1.55\times10^{-11}}{\sin^2 2\theta}\right), \tag{44}$$

if $m_{\nu\,\rm s}c^2/{\rm keV} \gtrsim 24$.

The current number density of sterile neutrinos $N_{\rm s,0}$ is proportional to the current number density of active neutrinos [$N_{\rm a} = 3N_{\rm b}(0)/(11\eta)$, where η is the baryon-to-photon density]. If we assume also that sterile neutrinos account for all the DM, we can write the number of sterile neutrinos per baryon as (cfr. Mapelli & Ferrara 2005)

$$n_{\rm s,0} = 5.88\times10^{5}\left(\frac{\rho_{\rm crit}}{10^{-29}\,{\rm g\,cm^{-3}}}\right)\left(\frac{\Omega_{\rm DM}}{0.198}\right) \times\left(\frac{m_{\nu\,\rm s}c^2}{8\,{\rm keV}}\right)^{-1}\left(\frac{\eta}{6.13\times10^{-10}}\right)^{-1}, \tag{45}$$

where $\rho_{\rm crit} \simeq 1.88\times10^{-29}h^2\,{\rm g\,cm^{-3}}$ is the critical density of the Universe.

Imposing $n_{\rm DM,0} = n_{\rm s,0}$ and $m_{\rm DM} = m_{\nu\,\rm s}$ we have all the ingredients needed to calculate $\dot{n}_{\rm DM}(z)$ through equation (36), for each considered mass.

Each sterile neutrino decay produces one active neutrino and one photon, each of them with an energy $\simeq(1/2)m_{\rm DM}c^2$. Since the active

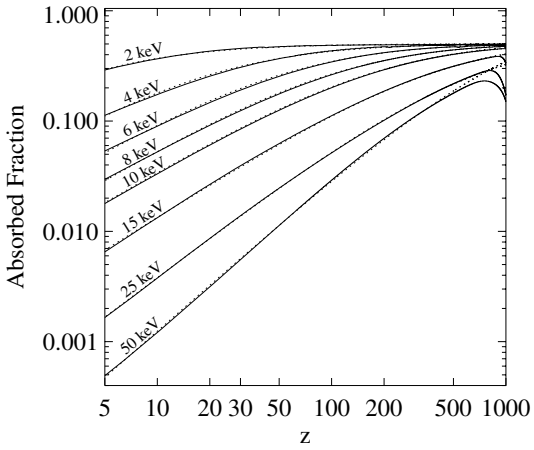

Figure 1. Absorbed fraction as a function of redshift for sterile neutrinos of masses between 2 and 50 keV (solid lines). The dotted lines, mostly superimposed to the solid ones, show the fitting functions listed in Appendix B. The decrease in $f_{\rm abs}$ which can be seen for $z \gtrsim 800$ for the 15, 25 and 50 keV curves might be an artefact caused by our choice of the redshift where the integration is started ($z_{\rm max} = 1100$), as is discussed in Appendix B.

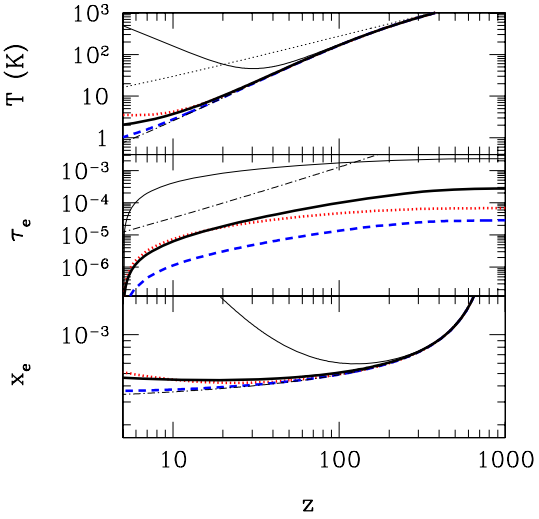

Figure 2. Ionized fraction (bottom panel), Thomson optical depth (central panel) and IGM temperature (top panel) as a function of redshift due to sterile neutrinos. The thick lines are obtained taking into account the effective absorbed fraction (Fig. 1) for sterile neutrinos of masses 4 (thick dotted line), 15 (dashed) and 25 keV (solid). The thin solid line shows the contribution of sterile neutrinos of mass 25 keV, if we assume an absorbed fraction $f_{\rm abs} = 0.5$. The thin dot–dashed line represents, from bottom to top, the relic fraction of free electrons, their contribution to Thomson optical depth and the IGM temperature without particle decays. In the top panel, the thin dotted line represents the CMB temperature.

neutrino does not interact with the IGM, we only need to consider the photon. Then, we use equations (10) and (11) with $\zeta_1 = 1$ and $\zeta_2 = 1/2$, in order to get the injection rate and average energy of photons, and proceed to the integration of equation (3).

The resulting absorbed fraction, $f_{\rm abs}(z)$, is shown in Fig. 1. In the case of complete and immediate absorption of the photon energy (i.e. the case studied by MFP06) $f_{\rm abs}(z)$ would be 0.5, because half of the sterile neutrino mass–energy is taken away by the active neutrino. It is clear that the complete absorption approximation is pretty good at high redshift, especially for low-mass sterile neutrinos ($m_{\nu,\,\rm s}c^2 \lesssim 4$ keV), whereas at low redshift it fails by a possibly large factor. In Appendix B, we provide analytical fits to the $f_{\rm abs}(z)$ curves shown above, for $3 \leqslant z \leqslant 1000$.

Implementing $\epsilon\,(z)$ in RECFAST (equations 38–40), we derive the effective influence of sterile neutrinos on the ionization fraction and IGM temperature (Fig. 2). The Thomson optical depth, $\tau_{\rm e}$, shown in Fig. 2 and in the following figures, has been calculated by integrating the well-known formula:

$$\tau_{\rm e} = \int_{z_1}^{z_2} {\rm d}z \frac{{\rm d}t}{{\rm d}z} c\sigma_{\rm T} x N_{\rm b}(z), \qquad (46)$$

where we take $z_2 = 1000$, i.e. the low-redshift boundary of the last scattering surface, and $z_1 = 5$, that is approximately the lowest redshift at which our fits of the absorbed fraction are valid (mostly because of our underlying assumption of a largely neutral IGM).

In Fig. 2, the solid thin line represents the effect of 25-keV neutrinos if we assume complete absorption by the IGM ($f_{\rm abs} = 0.5$ at every z), whereas the solid thick line was calculated using the derived absorbed fraction $f_{\rm abs}$. As could be expected from Fig. 1, the difference between the complete and the effective absorption cases (i.e. the thin and the thick line) increases as the redshift decreases. For instance, the ionization fraction in the total absorption case (thin line) is higher by a factor of $\sim$4 at $z = 20$, which becomes a factor of $\sim$24 at $z = 5$. The IGM temperature in the case of effective absorption $\epsilon\,(z)$ (thick line) is reduced by a significant factor ($\sim$235 at $z = 5$) with respect to the total absorption case. The Thomson optical depth is quite negligible, always remaining $<10^{-3}$.

In conclusion, accounting for the effective energy absorption significantly reduces the effect of sterile neutrino decays on reionization and heating, when compared to the case of total absorption (see MFP06).

The other two thick lines reported in Fig. 2 represent the effects of sterile neutrinos of 4 (dotted line) and 15 keV (dashed), using the derived absorbed fraction $f_{\rm abs}$. One can be surprised by the fact that 4-keV sterile neutrinos have a higher impact on ionization and heating than more massive neutrinos. This result comes from two different factors.

First of all, it depends on the fact that less massive sterile neutrinos have higher $f_{\rm abs}$, especially at low redshift. As one can see from the behaviour of $x_{\rm e}$ and $\tau_{\rm e}$, at high redshift 25-keV sterile neutrinos give a stronger contribution to ionization than 4-keV sterile neutrinos. It is only at $z \lesssim 20$ that this tendency is reversed.

The second reason is not 'physical', but it depends on the state of the art of observations. In fact, we adopted for each sterile neutrino mass the shortest lifetime consistent with observations. Present-day observational constraints happen to be much stronger for a 15-keV (Watson et al. 2006) than for a 25-keV sterile neutrino (Boyarsky et al. 2006a), independently of the intrinsic properties of the decay process.

3.2 Light dark matter

We define as light dark matter (LDM) particles all the DM candidates whose mass is between 1 and 100 MeV. Such particles have recently become of interest, because they provide a viable explanation for the detected 511-keV excess from the Galactic Centre (Knödlseder et al. 2005). If they are source of the 511-keV excess, then their maximum allowed mass $m_{\rm LDM}$ should be 20 MeV, not to overproduce detectable gamma-rays via internal Bremsstrahlung (Beacom, Bell & Bertone 2005). If we also consider the production of gamma rays for inflight annihilations of the positrons, this upper limit might become $\sim$3 MeV (Beacom & Yüksel 2006).

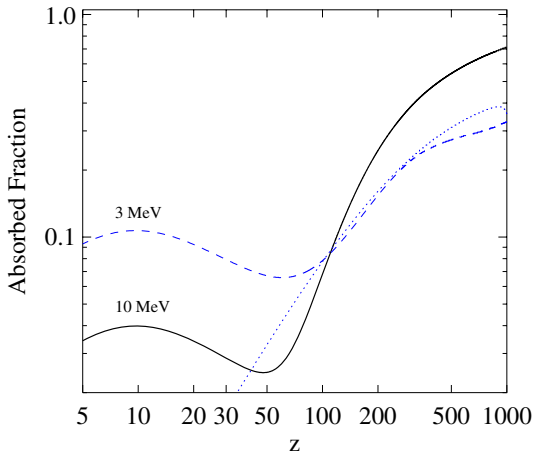

Figure 3. Absorbed fraction as a function of redshift for LDM particles of mass 3 (dashed line) and 10 MeV (solid line) decaying into pairs, and for LDM particles of mass 3 MeV (dotted line) decaying into photons.

In principle, LDM can both decay and annihilate, producing photons, neutrinos and pairs. We will treat both LDM decays and annihilations, making the assumption that the only decay/annihilation products are pairs. This represents quite an upper limit, because neutrinos do not interact with the IGM and MeV photons have a low probability to be significantly absorbed (see Fig. 3, and also the discussion in Chen & Kamionkowski 2004).

As we did for sterile neutrinos, we assume that LDM particles compose the entire DM. So the current number of LDM particles per baryon is

$$n_{\mathrm{LDM},0} = 4.46 \times 10^3 \left(\frac{\rho_{\mathrm{crit}}}{10^{-29}\,\mathrm{g\,cm^{-3}}}\right)\left(\frac{\Omega_{\mathrm{DM}}}{0.198}\right) \times \left(\frac{m_{\mathrm{LDM}}c^2}{1\,\mathrm{MeV}}\right)^{-1}\left[\frac{N_{\mathrm{b}}(0)}{2.5\times10^{-7}\,\mathrm{cm^{-3}}}\right]^{-1}, \quad (47)$$

where m_{LDM} is the mass of a LDM particle.

3.2.1 *Decays*

The LDM lifetime can be derived by assuming that LDM decays produce the detected 511-keV emission from the Galactic Centre (Hooper & Wang 2004):

$$\tau_{\mathrm{DM}} \sim 4 \times 10^{26}\,\mathrm{s}\left(\frac{m_{\mathrm{LDM}}c^2}{\mathrm{MeV}}\right)^{-1}. \quad (48)$$

From equations (47) and (48) we can derive $\dot{n}_{\mathrm{DM}}(z)$, defined in equation (36).

We assume that LDM decays produce pairs. So, the parameters needed in equations (21) and (22) are $\zeta_1 = 1$ (each decay produces a single electron and a single positron) and $\zeta_2 = 1/2$. (Both the electron and the positron receive approximately half of the available energy.)

Having defined these values, we then found the rate of energy absorption per baryon, $\epsilon(z)$, by integrating equation (3). The corresponding energy absorption fraction f_{abs} is shown in Fig. 3, where the cases of $m_{\mathrm{LDM}}c^2 = 3$ and 10 MeV are shown (dashed and solid line, respectively).

In the case of pair production, the assumption of immediate and complete energy absorption corresponds to $f_{\mathrm{abs}} = 1$ at every redshift, because both the electron and the positron energy can be absorbed. The effective value f_{abs} is always significantly less than 1.

At high redshift ($z \gtrsim 100$–200), the absorbed fraction is relatively high (0.3–0.7, depending on the particle mass), and it is dominated by the inverse Compton scattering on to CMB photons and by the positron annihilation. In fact, positron annihilations contribute to f_{abs} only at high redshift, because both the annihilation rate (see equation 23) and the probability of absorption of the photons they produce (equation 26) scale as positive powers of the baryon density.

Furthermore, CMB photons at high redshift are sufficiently energetic to be scattered up to the ionization threshold, because $\langle E_\gamma \rangle \sim 30\,\mathrm{eV}\,(E/5\,\mathrm{MeV})^2[(1+z)/1001]$ (where $\langle E_\gamma \rangle$ is the average energy of the photon after inverse Compton scattering and E is the energy of the electron/positron). At lower redshift, the starting energies of CMB photons is lower, and the energy boost due to the inverse Compton is not sufficient to turn them into ionizing photons, so the absorbed fraction drops significantly.

At low redshift ($z \lesssim 50$), the absorbed fraction f_{abs} stabilizes, because collisional ionizations become dominant. However, $f_{\mathrm{abs}}(z < 50)$ is always $\sim$0.1 for 3-MeV particles, or $\sim$0.03–0.04 for 10-MeV particles. We derived a fit for the absorbed fraction, reported in Appendix B.

For completeness, Fig. 3 also shows the case of LDM decays producing an active neutrino and a photon (dotted line) for 3-MeV LDM particles. In this case, at high redshift ($z \gtrsim 100$), the absorbed fraction for the LDM radiative decay is quite similar to that for the decay into a pair (especially if $m_{\mathrm{LDM}} \lesssim 3$ MeV). However, at redshifts $z \lesssim 100$ f_{abs} drops to much lower values for photons than for pairs, regardless of m_{LDM}.

In Fig. 4 we show the effects of LDM decays on reionization and heating, both considering the energy absorption rate $\epsilon(z)$ (thick lines) and the upper limit of complete absorption (thin lines, $f_{\mathrm{abs}} = 1$). For LDM decays the difference between the two cases is important, even if less than for 25-keV sterile neutrinos. For example, if $m_{\mathrm{LDM}}c^2 = 10$ MeV, the ionization fraction (the IGM temperature) at $z \sim 5$ is a

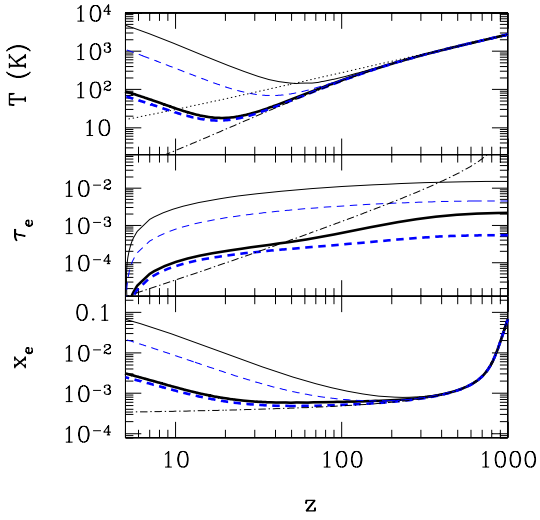

Figure 4. Ionized fraction (bottom panel), Thomson optical depth (central panel) and IGM temperature (upper panel) as a function of redshift due to LDM decays. The thick lines are obtained using the effective absorbed fraction (Fig. 3) for decaying LDM of masses 3 (thick dashed line) and 10 MeV (solid). The thin solid (dashed) line shows the contribution of decaying LDM of mass 10 (3) MeV, if we assume an absorbed fraction of 1. The thin dotted line in the top panel and the thin dot–dashed line in all the panels are the same as in Fig. 2.

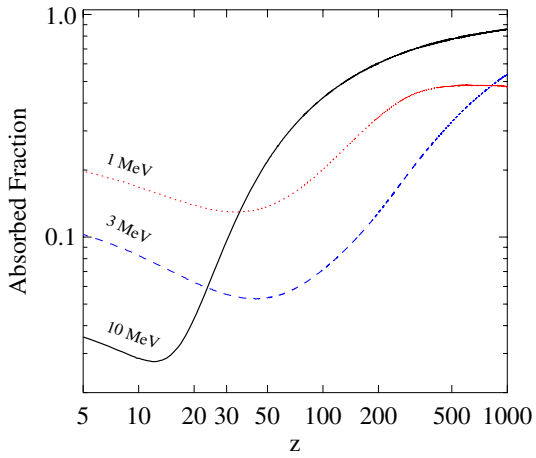

Figure 5. Absorbed fraction as a function of redshift for annihilating LDM of mass 1 (dotted line), 3 (dashed line) and 10 MeV (solid line).

factor of ∼23 (∼57) higher in the case of total absorption than if we consider our estimate of $f_{\rm abs}$. The Thomson optical depth is reduced by a factor of ∼7, and it is only $\tau_{\rm e} \lesssim 2.1 \times 10^{-3}$ (instead of $\tau_{\rm e} \lesssim 1.5 \times 10^{-2}$).

3.2.2 *Annihilations*

We now consider the case of LDM particles of mass $m_{\rm LDM}c^2 = 1$, 3 and 10 MeV, assuming that they annihilate and produce electron–positron pairs. Recently, Zhang et al. (2006) found that, in order to be consistent with the 1-yr *WMAP* results at the 1σ level, the thermally averaged annihilation cross-section for LDM annihilations must be[3]

$$\langle \sigma v \rangle \leqslant 2.2 \times 10^{-29}\ {\rm cm^3\ s^{-1}}\ f_{\rm abs}^{-1} \left(\frac{m_{\rm LDM}c^2}{\rm MeV} \right). \qquad (49)$$

The absorbed fraction $f_{\rm abs}$ depends on the redshift. However, as a conservative approximation, we take the value of $f_{\rm abs}$ in equation (49) to be the maximum value $f_{\rm abs,max}$ that we derive with our method (see Fig. 5). In particular, $f_{\rm abs,max} \simeq 0.5$ for 1 and 3-MeV LDM particles, and $f_{\rm abs,max} \simeq 0.9$ for 10-MeV particles; these values (and the whole function $f_{\rm abs}$) are actually independent from the value we adopt for $\langle \sigma v \rangle$.

We chose to use values of $\langle \sigma v \rangle$ which are close to the upper limit given by the above formula, i.e. 4, 12 and 24 $\times\ 10^{-29}$ cm^3 s^{-1} for $m_{\rm LDM}c^2$= 1, 3 and 10 MeV, respectively. Such values of $\langle \sigma v \rangle$ are quite close to those ($\langle \sigma v \rangle = 0.3$, 2.7 and 30 $\times\ 10^{-29}$ cm^3 s^{-1}, for the same masses) which have been inferred by Ascasibar et al. (2006) in order to reproduce the 511-keV excess from the Galactic Centre.

From equations (49) and (47) we then derive the rate of change of the number of DM particles per baryon through equation (37). In this case, the parameters for the injection equations (21) and (22) are $\zeta_1 = 1/2$, $\zeta_2 = 1$, because an electron and a positron are produced for every annihilation (which obviously involves two annihilating particles).

The integration of equation (3) with these parameters provides us with the energy absorption rate per baryon, $\epsilon(z)$, and the corresponding absorbed fraction $f_{\rm abs}$, which is shown in Fig. 5. The behaviour of $f_{\rm abs}(z)$ is quite similar to the case of LDM decays. At high redshift ($z \gtrsim 100$) $f_{\rm abs}(z)$ is close to the complete and immediate absorption value ($f_{\rm abs} = 1$) and it is dominated by inverse Compton scattering and positron annihilations. At low-redshift collisional ionizations alone contribute to $f_{\rm abs}$, which suffers a large drop between the two regimes.

We note that the contribution of positron annihilations to the absorbed fraction is particularly crucial for low-mass LDM particles. In fact, for the case $m_{\rm LDM}c^2 = 1$ MeV, inverse Compton scattering is not able to produce ionizing photons, even at $z \sim 1000$. For this reason, in absence of positron annihilation, the absorbed fraction for 1-MeV LDM particles (dotted line in Fig. 5) would depend only on collisional ionization, and its plot would essentially be a straight line from $f_{\rm abs}(5) \sim 0.2$ to $f_{\rm abs}(1000) \sim 0.08$.

On the contrary, for the highest mass we consider, $m_{\rm LDM}c^2 =$ 10 MeV, the high redshift bump is essentially due to inverse Compton energy loss.

The impact of LDM annihilations on reionization and heating (Fig. 6) is quite different from the case of LDM decays. In fact, LDM annihilations start to contribute both to reionization and heating already at very high redshift ($z \sim 800$); but their role remains negligible at low redshift. In particular, the ionization fraction becomes $\sim 10^{-3}$ and the IGM temperature at $z \sim 10$ is much lower than 10 K. This is mainly due to the fact that the annihilation rate depends on the square of the baryon density (see equation 37).

The Thomson optical depth reported in the central panel of Fig. 6 is quite high: $\tau_{\rm e} = 0.08$–0.10 for all the considered LDM particles, i.e. close to the best fit ($\tau_{\rm e} = 0.09$) of the 3-yr *WMAP* data. Nevertheless, the effects of LDM annihilations can be very hardly detected by *WMAP*. The reason is that, differently from the relatively rapid and large variation of the electron fraction occurring in standard reionization scenarios, the $x_{\rm e}$ evolution produced by LDM annihilations tracks very closely, albeit at a slightly higher level, and for a long time the relic abundance one. This behaviour dilutes the effects of

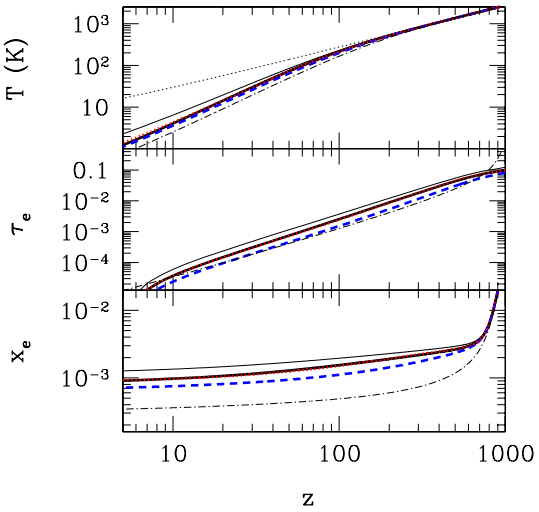

Figure 6. Ionized fraction (bottom panel), Thomson optical depth (central panel) and IGM temperature (upper panel) as a function of redshift due to LDM annihilations. The thick lines are obtained taking into account the effective absorbed fraction (Fig. 5) for annihilating LDM of masses 1 (thick dotted line), 3 (dashed) and 10 MeV (solid). The thin solid line shows the contribution of annihilating LDM of mass 10 MeV, if we assume an absorbed fraction = 1. The thin dotted line in the top panel and the thin dot–dashed line in all the panels are the same as in Fig. 2.

[3] In equation (49) the upper limit actually given by Zhang et al. (2006) was multiplied by a factor of 2 in order to account for differences between the two treatments.

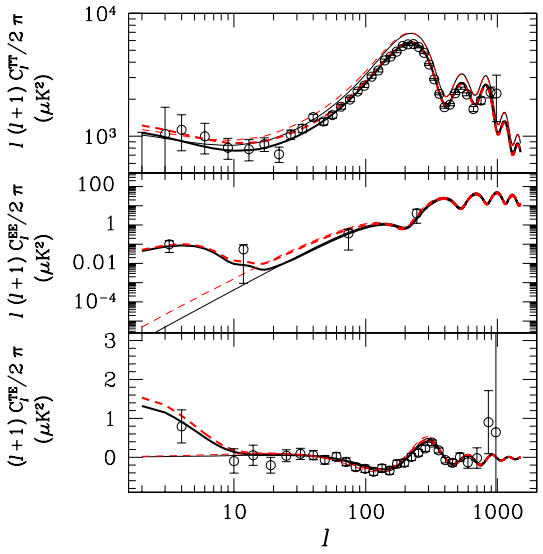

Figure 7. Temperature–temperature (top panel), polarization–polarization (central panel) and temperature–polarization (bottom panel) spectra. Thick lines indicate the CMB spectrum derived assuming Thomson optical depth $\tau_e = 0.09$ and a sudden reionization model (consistent with the 3-yr *WMAP* data); thin lines indicate the CMB spectrum derived assuming $\tau_e = 0$. Dashed (solid) lines indicate the CMB spectrum obtained (without) taking into account the annihilations of 1-MeV LDM particles. Open circles in all the panels indicate the 3-yr *WMAP* data (Hinshaw et al. 2006; Page et al. 2006; Spergel et al. 2006).

these extra electrons, making their imprint on the CMB spectrum very tiny, as can be appreciated from Fig. 7.

However, the Thomson optical depth produced by LDM annihilations should influence the CMB spectra at quite high multipoles, as implied by the results of Zhang et al. (2006). In Fig. 7 we show how annihilating LDM particles of mass 1 MeV modify the temperature–temperature (TT), polarization–polarization (EE) and temperature–polarization (TE) CMB spectra. The spectra have been simulated by running the public code CMBFAST (Seljak & Zaldarriaga 1996; Seljak et al. 2003), modified in order to account for the effects of DM decays/annihilations. The main effects of LDM annihilations are a certain damping in the TT peaks, a sensible variation of the EE spectra for $l \lesssim 100$ and some negligible distortions in the TE spectra. However, the simulated spectra agree within 1σ with the 3-yr *WMAP* results. Our plot is obtained assuming that all the cosmological parameters have the best-fitting value indicated by the 3-yr *WMAP* data. Leaving the cosmological parameters free to change, it should be possible to get an even better agreement between the *WMAP* data and the simulated CMB spectra derived accounting for LDM annihilations (Zhang et al. 2006).

4 CONCLUSIONS

We have modelled the absorption rate of the energy released in the IGM by DM decays/annihilations producing photons, electron–positron pairs and neutrinos. Our model suitably describes the energy deposition of a wide class of DM candidates, such as sterile neutrinos and LDM. Useful fits to the absorbed energy fraction as a function of redshift for the various particles are given in Appendix B.

In the case of radiatively decaying sterile neutrinos (mass 2–50 keV), at $z > 200$ a fraction $f_{abs} \simeq 0.5$ of the particle energy is transferred to the IGM, predominantly via ionizations; at lower redshifts f_{abs} decreases rapidly to values of 0.0005–0.3 depending on the neutrino mass. LDM particles can decay or annihilate. In both cases $f_{abs} \approx 1$ at high (> 300) redshift, due to positron annihilation and inverse Compton scattering, and it drops to values around 0.1 below $z = 100$.

Our determination of f_{abs} has a dramatic impact on the results of previous studies (which adopted naive assumptions for this parameter) concerned with the IGM heating by DM.

To illustrate this point, we have recalculated the IGM thermal and ionization history induced by either sterile neutrinos or LDM particles, using the previous findings. We find that sterile neutrino (LDM) decays are able to increase the IGM temperature by $z = 5$ at most up to 4 K (100 K). Both these values are 50–200 times lower than the estimates based on the assumption of complete energy transfer to the gas. In addition, significant departures from the adiabatic temperature evolution induced by the Hubble expansion occur only below $z \approx 30$, at an epoch when heating and ionization by conventional sources (stars or accretion-powered objects) are likely to swamp the DM signal.

LDM annihilations instead produce a very extended ($5 < z < 800$) electron fraction plateau, at a level of 5–10 times the relic one. The main effect of these extra electrons is to extend the cosmic time interval during which the IGM kinetic temperature is coupled to the CMB one down to $z \approx 100$. Although the electron scattering optical depth in this case is large (0.08–0.10), its effects on the CMB temperature/polarization spectra are hardly appreciable.

The detailed computation of the f_{abs} presented in this paper and summarized by the fits given in the Appendix B, might be useful for a large number of future applications in which the cosmological role of the DM is investigated. Among these are the effects of DM decays/annihilations on the 21-cm emission (Shchekinov & Vasiliev 2006) and on the structure formation history (Shchekinov & Vasiliev 2004; Biermann & Kusenko 2006; Ripamonti, Mapelli & Ferrara 2006).

ACKNOWLEDGMENTS

We thank S. Zaroubi, A. Kusenko, P. Biermann, J. Stasielak, C. Watson and X. Chen for useful discussions, and for detailed explanations about their results. We also thank the referee, Y. Ascasibar, for a careful reading of the manuscript and useful comments. ER (MM) thanks SISSA/ISAS (the Kapteyn Institute) for the hospitality during the preparation of this paper. ER gratefully acknowledges support from the Netherlands Organization for Scientific Research (NWO) under project number 436016.

REFERENCES

Abazajian K., 2006, Phys. Rev. D, 73f, 3506
Abazajian K., Koushiappas S. M., 2006, Phys. Rev. D, 74, 023 527
Abazajian K., Fuller G. M., Tucker W. H., 2001, ApJ, 562, 593
Ascasibar Y., Jean P., Boehm C., Knödlseder J., 2006, MNRAS, 368, 1695
Beacom J. F., Yüksel H., 2006, Phys. Rev. Lett., 97g, 1102
Beacom J. F., Bell N. F., Bertone G., 2005, Phys. Rev. Lett., 94q, 1301
Biermann P. L., Kusenko A., 2006, Phys. Rev. Lett., 96L, 1301
Boehm C., Hooper D., Silk J., Casse M., Paul J., 2004, Phys. Rev. Lett., 92j, 1301
Boyarsky A., Neronov A., Ruchayskiy O., Shaposhnikov M., 2006a, MNRAS, 370, 213
Boyarsky A., Neronov A., Ruchayskiy O., Shaposhnikov M., 2006b, Phys. Rev. D., 74, 103506

Cassé M., Fayet P., 2006, in Mamon G., Combes F., Deffayet C., Fort B., eds, Proc. 21st IAP Colloq., European Astronomical Society, Publ. Ser. Vol. 20, Mass Profiles and Shapes of Cosmological Structures. EAS, Paris, p. 201
Chen X., Kamionkowski M., 2004, Phys. Rev. D, 70d, 3502
Colombi S., Dodelson S., Widrow L. M., 1996, ApJ, 458, 1
Furlanetto S., Pritchard J. R., 2006, MNRAS, 372, 1093
Hansen S. H., Haiman Z., 2004, ApJ, 600, 26
Hinshaw G. et al., 2006, ApJ, submitted (astro-ph/0603451)
Hooper D., Wang L.-T., 2004, Phys. Rev. D, 70f, 3506
Kasuya S., Takahashi F., 2005, Phys. Rev. D, 72h, 5015
Kawasaki M., Yanagida T., 2005, Phys. Lett. B, 624, 162
Knödlseder J. et al., 2005, A&A, 441, 513
Lang K. R., 1999, Astrophysical Formulae, 3rd edn. Springer-Verlag, Berlin
Longair M. S., 1992, High Energy Astrophysics, Vol. 1, 2nd edn. Cambridge Univ. Press, Cambridge
Mapelli M., Ferrara A., 2005, MNRAS, 364, 2
Mapelli M., Ferrara A., Pierpaoli E., 2006, MNRAS, 369, 1719 (MFP06)
Padmanabhan T., 1995, Structure Formation in the Universe. Cambridge Univ. Press, Cambridge
Padmanabhan N., Finkbeiner D. P., 2005, Phys. Rev. D, 72b, 3508
Page L. et al. 2006, ApJ, submitted (astro-ph/0603450)
Peskin M. E., Schroeder D. V., 1995, An Introduction to Quantum Field Theory. Addison-Wesley, Reading, chap. 6
Picciotto C., Pospelov M., 2005, Phys. Lett. B, 605, 15
Pierpaoli E., 2004, Phys. Rev. Lett., 92, 031 301
Ripamonti E., Mapelli E., Ferrara A., 2006, MNRAS, submitted (astro-ph/0606483)
Rybicki G. B., Lightman A. P., 1979, Radiative Processes in Astrophysics. Wiley, New York
Seager S., Sasselov D. D., Scott D., 1999, ApJ, 523, L1
Seager S., Sasselov D. D., Scott D., 2000, ApJS, 128, 407
Seljak U., Zaldarriaga M., 1996, ApJ, 469, 437
Seljak U., Sugiyama N., White M., Zaldarriaga M., 2003, Phys. Rev. D, 68h, 3507
Seljak U., Makarov A., McDonald P., Trac H., 2006, Phys. Rev. Lett., 97, 191303
Shaposhnikov M., 2006, CERN-PH-TH/2006-079
Shchekinov Y. A., Vasiliev E. O., 2004, A&A, 419, 19
Shchekinov Y. A., Vasiliev E. O., 2006, MNRAS, submitted (astro-ph/0604231)
Shull J. M., van Steenberg M. E., 1985, ApJ, 298, 268
Sommer-Larsen J., Dolgov A., 2001, ApJ, 551, 608
Spergel D. N. et al., 2006, ApJ, submitted (astro-ph/0603449)
Viel M., Lesgourgues J., Haehnelt M. G., Matarrese S., Riotto A., 2005, Phys. Rev. D, 71, 3534
Viel M., Lesgourgues J., Haehnelt M. G., Matarrese S., Riotto A., 2006, Phys. Rev. Lett., 97g, 1301
Watson C. R., Beacom J. F., Yüksel H., Walker T. P., 2006, Phys. Rev. D, 74c, 3009
Zdziarski A. A., Svensson R., 1989, ApJ, 344, 551 (ZS89)
Zhang L., Chen X., Lei Y.-A., Si Z., 2006, Phys. Rev. D, submitted (astro-ph/0603425)

APPENDIX A: INTERNAL BREMSSTRAHLUNG

In Section 2.2 we have considered the energy losses of electrons and positrons produced by DM decays or annihilations. However, because of the so-called *internal Bremsstrahlung* process, it is possible that an annihilation results in the production of an electron–positron pair, plus a photon (Beacom, Bell & Bertone 2005). As the photon carries away a fraction of the energy released by the annihilation, this mechanism could influence $f_{\rm abs}$.

We can estimate the fraction of energy carried away by the photons produced by internal Bremsstrahlung by using the cross-section reported in Beacom et al. (2005):

$$\frac{{\rm d}\sigma_{\rm Br}}{{\rm d}E} = \sigma_{\rm tot}\frac{\alpha}{\pi}\frac{1}{E}\left[\ln\left(\frac{s'}{m_{\rm e}^2c^4}\right)-1\right]\left[1+\left(\frac{s'}{s}\right)^2\right], \tag{A1}$$

where E is the energy of the photon, $\sigma_{\rm tot}$ is the total annihilation cross-section in the three-level approximation (Peskin & Schroeder 1995), α is the fine structure constant, $s = 4(m_{\rm DM}c^2)^2$ and $s' = 4m_{\rm DM}c^2(m_{\rm DM}\,c^2 - E)$.
Then, the fraction of the annihilation energy which is carried away by the photons is

$$f_{\rm Br} = \frac{1}{2\sigma_{\rm tot}m_{\rm DM}c^2}\int_0^{m_{\rm DM}c^2}\frac{{\rm d}\sigma_{\rm Br}}{{\rm d}E}E\,{\rm d}E \;\leqslant\; \frac{2\alpha}{\pi}\ln(2m_{\rm DM}/m_{\rm e}), \tag{A2}$$

where we have exploited the fact that

$$\frac{{\rm d}\sigma_{\rm Br}}{{\rm d}E} \leqslant \sigma_{\rm tot}\frac{4\alpha}{\pi}\frac{\ln(2m_{\rm DM}/m_{\rm e})}{E}. \tag{A3}$$

So, even for the highest mass we consider ($m_{\rm DM} = 10\,{\rm MeV}$), $f_{\rm Br} \leqslant 0.017$. Such a fraction is small; but, if the internal Bremsstrahlung photons were completely absorbed, it is enough to significantly alter the value of $f_{\rm abs}$ at low redshift, at least for 10-MeV LDM annihilations (see Fig. 5).

However, this is not the case: the typical energy of a photon produced by the internal Bremsstrahlung mechanism is $\sim(1/2)m_{\rm DM}c^2$, and equation (26) can be used in order to estimate the optical depth encountered by such a photon for each Hubble length it travels. For the 5 MeV photons typically produced by the annihilations of 10-MeV LDM particles this is $\tau \simeq 2.2\times10^{-4}\,(1+z)^{3/2}$, so that the complete absorption scenario is realistic only for $z \gtrsim 150$, when $f_{\rm Br} \ll f_{\rm abs}$. Then, it is justified to neglect the internal Bremsstrahlung process in estimating $f_{\rm abs}$.

APPENDIX B: FITS OF THE ABSORBED ENERGY FRACTION

It can be useful to derive a fit of the energy absorbed fraction ($f_{\rm abs}$) for each considered DM particle. We calculated fits with errors smaller than 5 per cent for $5 \lesssim z \lesssim 1000$. In the redshift range $3 \lesssim z \lesssim 5$ the errors are larger ($\lesssim$10–20 per cent); however, at such low redshift our absorbed fractions are likely inaccurate by a larger factor, as our assumption of a mostly neutral IGM breaks down.

B1 Sterile neutrinos

For the case of sterile neutrino with mass $2 \leqslant m_{\nu,\mathrm{s}}c^2/\mathrm{keV} \leqslant 10$, a fit was found depending only on the redshift and the mass of the particle:

$$f_{\mathrm{abs}}(z, m_{\nu,\mathrm{s}}) = \left[0.5 + 0.032\left(\frac{m_{\nu,\mathrm{s}}c^2}{8\,\mathrm{keV}}\right)^{1.5}\right]\left[\frac{z}{110\left(\frac{m_{\nu,\mathrm{s}}c^2}{8\,\mathrm{keV}}\right)^{2.4} + z}\right]^{0.93}. \tag{B1}$$

This general formula does not hold for higher masses, for which we have found

$$\begin{aligned}
f_{\mathrm{abs}}(z, 15\,\mathrm{keV}) &= 0.99\left[0.5 + 0.032\left(\frac{15\,\mathrm{keV}}{8\,\mathrm{keV}}\right)^{1.5}\right]\left[\frac{z}{110\left(\frac{14\,\mathrm{keV}}{8\,\mathrm{keV}}\right)^{2.4} + z}\right]^{1.0},\\
f_{\mathrm{abs}}(z, 25\,\mathrm{keV}) &= 0.89\left[0.5 + 0.032\left(\frac{25\,\mathrm{keV}}{8\,\mathrm{keV}}\right)^{1.5}\right]\left[\frac{z}{110\left(\frac{17\,\mathrm{keV}}{8\,\mathrm{keV}}\right)^{2.4} + z}\right]^{1.2},\\
f_{\mathrm{abs}}(z, 50\,\mathrm{keV}) &= 1.08\left[0.5 + 0.032\left(\frac{50\,\mathrm{keV}}{8\,\mathrm{keV}}\right)^{1.5}\right]\left[\frac{z}{110\left(\frac{22\,\mathrm{keV}}{8\,\mathrm{keV}}\right)^{2.4} + z}\right]^{1.4}.
\end{aligned} \tag{B2}$$

As can be seen in Fig. 1, these last fits do not take into account the decrease of f_{abs} at very high redshift, which is caused by the fact that we start integrating equation (3) at redshift 1100. In fact, if we start the integration at $z = 1500$, the high redshift discrepancies between the fitting formulae above and the actual f_{abs} disappear; however, such a procedure is uncertain because the equations we use for describing the energy absorption might not be applicable at an epoch before recombination.

Luckily, the energy injection from sterile neutrino decays is completely negligible at such high redshift, and this uncertainty by a factor $\lesssim 2$ can be safely ignored.

B2 Light dark matter

For LDM particles decaying into pairs, we derived two different fits, for 3- and 10-MeV particles, respectively:

$$\begin{aligned}
f_{\mathrm{abs}}(z, 3\,\mathrm{MeV}) &= 0.49(1+z)^{-0.5}\exp\left[-\left(\frac{5}{1+z}\right)^{1.4}\right]\\
&\quad + 0.058(1+z)^{0.28}\exp\left[-\left(\frac{164}{1+z}\right)^{1.4}\right] - 0.265\exp\left[-\left(\frac{1220}{1+z}\right)^{1.4}\right],\\
f_{\mathrm{abs}}(z, 10\,\mathrm{MeV}) &= 0.21\,(1+z)^{-0.55}\exp\left[-\left(\frac{5.1}{1+z}\right)^{1.4}\right] + 0.222\,(1+z)^{0.18}\exp\left[-\left(\frac{185}{1+z}\right)^{1.36}\right].
\end{aligned} \tag{B3}$$

Finally, for annihilating LDM particles, we derived the following fits:

$$\begin{aligned}
f_{\mathrm{abs}}(z, 1\,\mathrm{MeV}) &= 0.32(1+z)^{-0.27} + 0.55(1+z)^{0.06}\exp\left[-\left(\frac{195}{1+z}\right)^{0.9}\right]\exp\left[-\left(\frac{1+z}{1900}\right)^{1.2}\right],\\
f_{\mathrm{abs}}(z, 3\,\mathrm{MeV}) &= 0.21(1+z)^{-0.39} + 0.155(1+z)^{0.20}\exp\left[-\left(\frac{350}{1+z}\right)^{0.7}\right]\\
&\quad + 2.9\times 10^{-4}\,(1+z)\exp\left(-\frac{550}{1+z}\right),\\
f_{\mathrm{abs}}(z, 10\,\mathrm{MeV}) &= 0.064\,(1+z)^{-0.34} + 0.335\,(1+z)^{0.14}\exp\left[-\left(\frac{52}{1+z}\right)^{1.3}\right].
\end{aligned} \tag{B4}$$

This paper has been typeset from a TEX/LATEX file prepared by the author.